Mapping global forest age from forest inventories, biomass and climate data

Simon Besnard[1,2], Sujan Koirala[1], Maurizio Santoro[5], Ulrich Weber[1], Jacob Nelson[1], Jonas Gütter[1,4], Bruno Herault[6,7], Justin Kassi[8], Anny N'Guessan[8], Christopher Neigh[9], Benjamin Poulter[9], Tao Zhang[10,11], Nuno Carvalhais[1,3]

[1]Max Planck Institute for Biogeochemistry, Germany

[2]Laboratory of Geo-Information Science and Remote Sensing, Wageningen University & Research, The Netherlands

[3]Departamento de Ciências e Engenharia do Ambiente, DCEA, Faculdade de Ciências e Tecnologia, FCT, Universidade Nova de Lisboa, Portugal

[4]DLR, Institute of Data Science Data Management and Analysis, Germany

[5]Gamma Remote Sensing, Switzerland

[6]INP-HB, Institut National Polytechnique Félix Houphouët-Boigny, Côte d'Ivoire

[7]Cirad, University of Montpellier, UR Forests & Societies, France

[8]Université Félix Houphouët-Boigny, UFR Biosciences, Laboratoire de Botanique, Côte d'Ivoire

[9]NASA Goddard Space Flight Center, Biospheric Sciences Lab., Greenbelt, MD, USA

[10]University of Florida, Department of Biology, United States

[11]University of Minnesota, Department of Forest Resources, United States

Correspondence to: Simon Besnard (sbesnard@bgc-jena.mpg.de) and Nuno Carvalhais (ncarvalhais@bgc-jena.mpg.de)

Abstract. Forest age can determine the capacity of a forest to uptake carbon from the atmosphere. However, a lack of global diagnostics that reflect the forest stage and associated disturbance regimes hampers the quantification of age-related differences in forest carbon dynamics. This study provides a new global distribution of forest age circa 2010, estimated using a machine learning approach trained with more than 40,000 plots using forest inventory, biomass and climate data. First, an evaluation against the plot level measurements of forest age reveals that the data-driven method has a relatively good predictive capacity of classifying old-growth vs. non-old-growth (precision = 0.81 and 0.99 for old-growth and non-old-growth, respectively) forests and estimating corresponding forest age estimates (NSE = 0.6 and RMSE = 50 years). However, there are systematic biases with overestimation in young and underestimation in old forest stands, respectively. Globally, we find a large variability of forest age with the old-growth forests in the tropical regions of Amazon and Congo, young forests in China and intermediate stands in Europe. Furthermore, we find that the regions with high rates of deforestation or forest degradation (e.g., the arc of deforestation in the Amazon) are composed mainly of younger stands. Assessment of forest age in the climate-space shows that the old forests are either in cold and dry regions or warm and wet regions, while young-intermediate forests span a large climatic gradient. Finally, comparing the presented forest age estimates with a series of regional products reveals differences rooted in different approaches and different *in-situ* observations and global-scale products. Despite showing robustness in cross-validation results, additional methodological insights on further developments should as much as possible harmonize data across the different approaches. The forest age dataset presented here provides additional insights into the global distribution of forest age to better understand the global dynamics in the forest water and carbon cycles. The forest age datasets are openly available at https://doi.org/10.17871/ForestAgeBGI.2021 (Besnard et al., 2021).

1 Introduction

Forests cover about 30% of the terrestrial surface of our planet and store a large part of the ~~terrestrial~~ carbon, indicating their fundamental role in the ~~terrestrial~~ carbon cycle (Bar-On et al., 2018). However, drivers controlling the capacity of the terrestrial biosphere to sequester carbon remain poorly characterized, limiting our understanding of the global land carbon sink's location (Cook-Patton et al., 2020). Such uncertainties on the geographical distribution of the carbon sink have been partly attributed to the fact that forest regrowth and demography are not systematically considered for understanding changes in the forest carbon sink (Pugh et al., 2019; Zscheischler et al., 2017).

While the recent increase in the forest carbon sink is controlled by environmental changes such as carbon dioxide (CO_2) fertilization, nitrogen deposition, and climate change (Zhu et al., 2016; Winkler et al., 2021), the forest carbon balance dynamics are also attributed to disturbance history and forest regrowth (Besnard et al., 2018; Pugh et al., 2019; Amiro et al., 2010). Forest disturbances cause physical damages to vegetation properties and changes in forest demography, thereby affecting the balance of terrestrial CO_2 exchange with the atmosphere by temporarily increasing respiration and reducing photosynthesis (Birdsey et al., 2006; Johnson and Curtis, 2001; Liu et al., 2011; Williams et al., 2012; Woodbury et al., 2007). The changes in the strength of carbon uptake or release can alter the forest carbon balance by converting forest ecosystems from carbon sinks to sources (Amiro et al., 2010; Bowman et al., 2009; Ciais et al., 2014; Moore et al., 2013). (Odum, 1969) hypothesized the first theory to describe the ecosystem development in the absence of significant disturbance, suggesting that the age of forests and demographic changes drive carbon accumulation. Nevertheless, stand age distribution can be modified to varying degrees of changes in environmental conditions and

disturbance, therefore slowly change along with stand age or successional continuum (Irvine et al., 2005; Piponiot et al., 2018).

Despite the sensitivity of the forest carbon balance to disturbance and regrowth (Buitenwerf et al., 2018; Sulla-Menashe et al., 2018), existing empirical models and current bottom-up spatiotemporal assessment of CO_2 fluxes do not explicitly account for these effects (Jung et al., 2011; Tramontana et al., 2016; Jung et al., 2020). The forest carbon balance in regions with newly disturbed and old-growth forests may not be realistically estimated by not explicitly constraining data-driven statistical models with disturbance history or forest demography. For instance, large discrepancies are observed between bottom-up statistical approaches (e.g., FLUXCOM initiatives, http://www.fluxcom.org/) and atmospheric inversions in estimating net ecosystem exchange (NEE), particularly in the tropics where site history plays a substantial role in NEE magnitude (Pugh et al., 2019). To account for the contribution of disturbance on the land carbon sink, we need information on the geographical distribution of disturbance, albeit such information is somewhat limited at the global scale (Ciais et al., 2014). Forest age, related to time since disturbance, can be seen as a useful surrogate in analyzing the impact of disturbance on the ability of forests to store carbon. Incorporating forest age into terrestrial biosphere modelling offers a starting point to characterize disturbance history, so getting more insights into the location of the terrestrial carbon sinks (Pugh et al., 2019). Reliable estimates of forest age at the global-scale are, therefore, an essential and needed source of information. The recent advances in describing the geographical distribution of forest demography globally (Huang et al., 2010; Kennedy et al., 2010; Poulter et al., 2019) have paved the way to consider forest age and disturbance history in carbon cycle studies.

Here, we aim to provide a new gridded global forest age dataset *circa* 2010 inferred from a compilation of forest inventory, biomass and climate data. More specifically, we introduce the *in-situ* forest inventory dataset, the modelling framework used in this study and the predictive capacity of the presented model to estimate forest age at the plot level. We further describe the global and regional patterns of the forest age product and their uncertainties. The presented forest age dataset is finally benchmarked against a series of independent regional and global datasets.

2 Method

2.1 Forest inventory and climate data

The globally gridded forest age dataset was developed by collecting *in-situ* plot level stand age and aboveground biomass (AGB) estimates from a series of forest inventory databases (Álvarez-Dávila et al., 2017; Anderson-Teixeira et al., 2018; Anderson-Teixeira et al., 2016; Baker et al., 2016; Johnson et al., 2016; Lewis et al., 2013; Mitchard et al., 2014; N'Guessan et al., 2019; Poorter et al., 2016; Schepaschenko et al., 2017; Somogyi et al., 2008; Sullivan et al., 2017). Besides, we sampled 20,000 observations from the US Forest Service Forest Inventory and Analysis (FIA) data (Burill et al. 2018) containing i*n-situ* plot level stand age and aboveground biomass (AGB) estimates (the original number of observations in the FIA dataset = 350,000). To reduce the unbalanced sample size across age classes, we weight-sampled the FIA data with decadal age classes underrepresented in the dataset before including the FIA data having higher weights. The weights for each decadal class were calculated following Eq. (1):

$$weight_i = \frac{1}{n} \sum_{i=1}^{n} N\,age\,class_i \quad (1)$$

Where i is a decadal class and n is the number of observations.

The methods used in inventory surveys to estimate stand age relied on expert knowledge, tree diameter measurements, tree rings from cores of selected trees (e.g., Burill et al. 2018), or semi-directive interviews (e.g., (N'Guessan et al., 2019)). Forest inventory plots were classified as old-growth forests when stand age was more than or equal to 300 years. In total, the final dataset had around 25,000 plots and around 44,000 observations. Geographical biases were observed in the compiled dataset (Fig. 1), with North America, Europe and South East of China being well represented, while Africa, Indonesia, and Australia were either underrepresented or not represented. The Amazon basin and the West part of Eurasia were relatively well represented. Besides, stand age data were generally collected in locations easily accessible; therefore, unmanaged forests in remote areas were very likely less represented than managed forests.

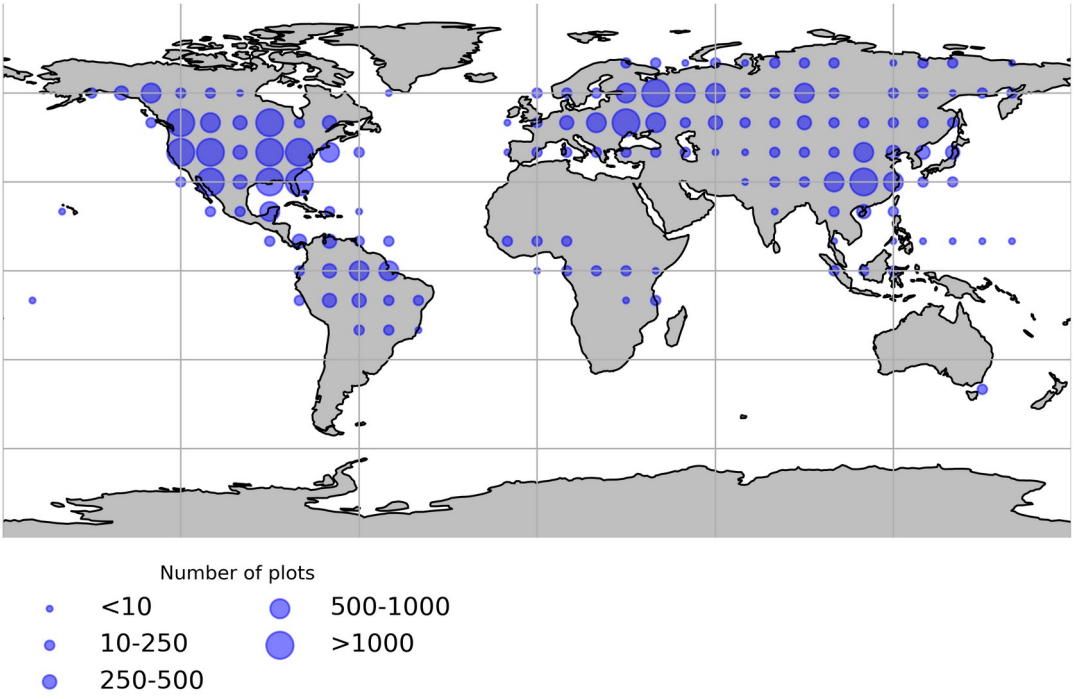

Figure 1 Spatial distribution of the forest inventory plots used for the forest age maps. Each dot represents the total number of plots within 10x10 degrees.

A comprehensive meta-analysis of the compiled dataset (Fig. 2) revealed that the observations covered a large spectrum in the climate-space (Fig. 2A), although there were few plots in hot and dry regions, likely due to the low presence of forest ecosystems in such regions. We further described the age spectrum covered at the regional scale and found that a large spectrum of forest age was covered in North America (Fig. 2B) and Eurasia (Fig. 2C), while in the tropics, biases were observed (i.e., a significant fraction of tropical old-growth forest and relatively young forests) (Fig. 2D).

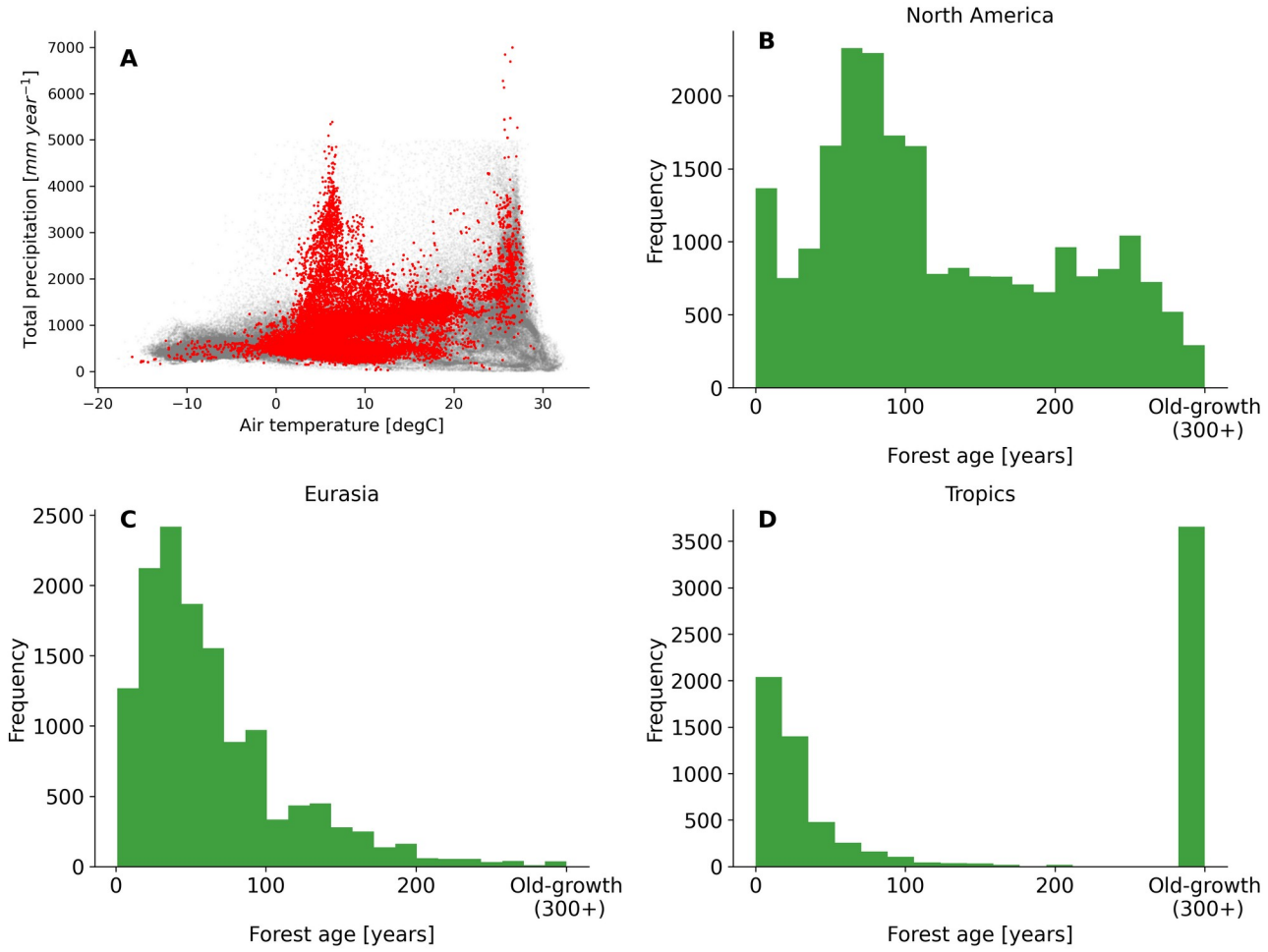

Figure 2 Distribution of the forest inventory plots in a climate space defined by air temperature and total annual precipitation (A). Histogram distributions of the forest age observations in North America (B), Eurasia (C) and the tropics (D) are also shown. The grey dots show the global distribution of 0.25° grid-cell forest in climate space defined by air temperature and precipitation, while the red dots show the distribution of the forest inventory data in the same climate space.

For each forest inventory plot, we extracted bioclimatic variables from the WorldClim version2 (Fick and Hijmans, 2017). In addition, we extracted all the soil-related variables of the Harmonized World Soil Database v 1.2 dataset. Finally, we derived a series of proxies for disturbance and management regimes from the Hansen tree cover dataset (Hansen et al., 2013):

- The intensity of tree loss from the Hansen tree cover loss layer. This metric was derived by counting the 30m pixels that experienced a tree cover loss for 2000-2019 within a 1km gridcell.
- Last time since tree cover loss from Hansen tree cover loss layer – standard deviation metric. This metric was calculated as the last time from 2019 since a 30m pixel experienced tree cover loss, and we further computed the standard deviation of this last time since tree cover loss within a 1km gridcell.

Table S1 summarizes the list of covariates considered in our study. Two datasets were further created. First, we created a dataset that contained the plots with a reported stand age estimates ranging from 1 to 299 years (hereafter non-old-

growth forests dataset). Second, we created a binary dataset reporting whether an observation had an age estimate less than 300 years old or whether an observation had an age estimate more than or equal to 300 years old or not reported but considered as old-growth tropical forests (0= non-old-growth forest and 1= old-growth forest) (hereafter old-growth forests dataset).

2.2 Feature selection and model training

From the set of predictors related to vegetation and climatic conditions (Table S1), we performed a feature ranking with recursive feature elimination (RFE) procedure (https://scikit-learn.org/stable/modules/generated/sklearn.feature_selection.RFE.html) (Guyon et al., 2002) both on the non-old-growth forest and old-growth datasets. The ten best covariates selected by the RFE algorithm were further used to train either a Random Forest (RF) regressor algorithm (RFregressor) (https://scikit-learn.org/stable/modules/generated/sklearn.ensemble.RandomForestRegressor.html) or an RF classifier algorithm (Rfclassifier (https://scikit-learn.org/stable/modules/generated/sklearn.ensemble.RandomForestClassifier.html). As such, two distinct models were implemented. The RFregressor model was used to estimate forest age in the non-old-growth forests dataset, while the RFclassifier model was used to classify old-growth vs. non-old-growth forests using the old-growth forests dataset. The performances of the two models were assessed using leave-one-cluster-out cross-validation to reduce possible spatial auto-correlation between the training and test sets (Ploton et al., 2020). A cluster of plots contained all the plots within the same pair of latitude and longitude coordinates rounded to the nearest 10th degree (e.g., latitude= 20 degrees and longitude= 110 degrees) (see Fig. 1). For the RFregressor model, the root-mean-square error (RMSE), the normalized root-mean-square error (NRMSE) and Nash-Sutcliffe model efficiency coefficient (NSE) were used for assessing the predictive capacity of the model for predicting forest age. For the RFclassifier model, we reported the precision (i.e., the number of correctly-identified members of a class divided by all the times the model predicted that class), recall (i.e., the number of members of a class that the classifier identified correctly divided by the total number of members in that class) metrics, and F1-score (i.e., the combination of precision and recall). Additionally, we explored functional relationships between the variables selected by the feature selection procedure and stand age in the RFregressor model by using the Tree SHapley Additive exPlanations (TreeSHAP) algorithm (Lundberg and Lee, 2017; Lundberg et al., 2019). A negative SHAP value for a given variable X translates a negative contribution to the local changes of forest age and vice-versa.

2.3 Upscaling procedure

To upscale the two trained models (i.e., RFclassifier and RFregressor models) from plot-level data to the global scale, we collected climate grids from the WorldClim dataset (Fick and Hijmans, 2017)(Fick and Hijmans, 2017) and a series of AGB grids *circa* 2010 (i.e., corrected for tree cover with thresholds of 0%, 10%, 20% and 30%) from the Globbiomass project (http://globbiomass.org/) (Santoro et al., 2021). The tree cover correction was done by masking out the 100-meter pixels in the original AGB product (i.e., 100m resolution) having tree cover estimates (Hansen et al., 2013) below one of the tree cover thresholds mentioned above within a 1km extent. The original filtered AGB maps were aggregated from 100m to 1km spatial resolution with a bilinear resampling method.

The upscaling procedure was done in two steps. First, each 1km pixel was classified as old-growth or non-old growth forests using the trained RFclassifier model. Second, the 1km pixels classified as non-old growth were assigned with an age estimate ranging from 0-299 years inferred from the RFregression model, while the pixels classified as old-growth forest were assigned a default age value of 300 years. In total, four gridded forest age maps with a 1km spatial resolution were obtained using the different AGB maps derived from the different tree cover thresholds as mentioned above (hereafter MPI-BGC forest age datasets). We also created maps from the 1km resolution forest age maps that reflected the fraction of several age classes (0-300+ with decadal resolution) within each 0.5-degree grid cell resolution.

3 Results and discussion

3.1 Model development and evaluation

We used the ten most important variables from the set presented in Table S1 identified by the RFE algorithm procedure for the RFregression and the RFclassifier models (Table 1). This set of selected variables was further used to train the two models in the cross-validation analysis and the global upscaling procedure.

Table 1 List of the predictors confirmed as important by the feature selection algorithm for RFregression and the RFclassifier models. See table S1 for details on the variable names.

Model setup	Vegetation variables	Hydro-meteorological variables
RFregression	agb	Isothermality, MaxTemperatureofWarmestMonth, MeanDiurnalRange, MeanTemperatureofWettestQuarter, PrecipitationofWarmestQuarter, PrecipitationofWettestMonth, PrecipitationSeasonality, srad, vapr
RFclassifier	agb	AnnualMeanTemperature, AnnualPrecipitation,Isothermality, MeanTemperatureofColdestQuarter, MeanTemperatureofDriestQuarter, MinTemperatureofColdestMonth, TemperatureAnnualRange, TemperatureSeasonality, vapr

By assessing the cross-validation results, we found that the RFclassifier model could accurately partition old-growth and non-old-growth forests with precision estimates of 0.81 and 0.99 for old-growth and non-old-growth forests, respectively (Fig. 3A). Furthermore, we found recall values of 0.94 and 0.98 for old-growth and non-old-growth forests, respectively, while we found F1-scores of 0.87 and 0.99 for old-growth and non-old-growth forests, respectively (Fig. 3A). The performance of the RFregression model was relatively high (NSE= 0.60, RMSE= 47.63 years and NRMSE = 51.52%) (Fig. 3B), while the model residuals across 10-degree latitudinal averages were relatively low (Fig. 3C). However, the quantile-quantile plot depicted biases in both very young and old forests (Fig. 3D). More precisely, the RFregression model slightly overestimated the age estimates of young forests while underestimating the age estimates of older forests (i.e., >150 years old) at the plot level. The biases for the very young or the older forests were possibly

due to the properties of the training dataset in which older forests are still largely underrepresented compared to younger stands (Fig. 2A-C) (i.e., skewed distribution of the age estimates). Such biases could potentially be propagated from plot level to global scale and have implications in representing the location of younger and older forests globally. Figure 3E shows the spatial patterns of the model residuals. For instance, we observed that the RFregression model underestimated the age estimates in most North American forests while overestimated the age estimates in most European forests.

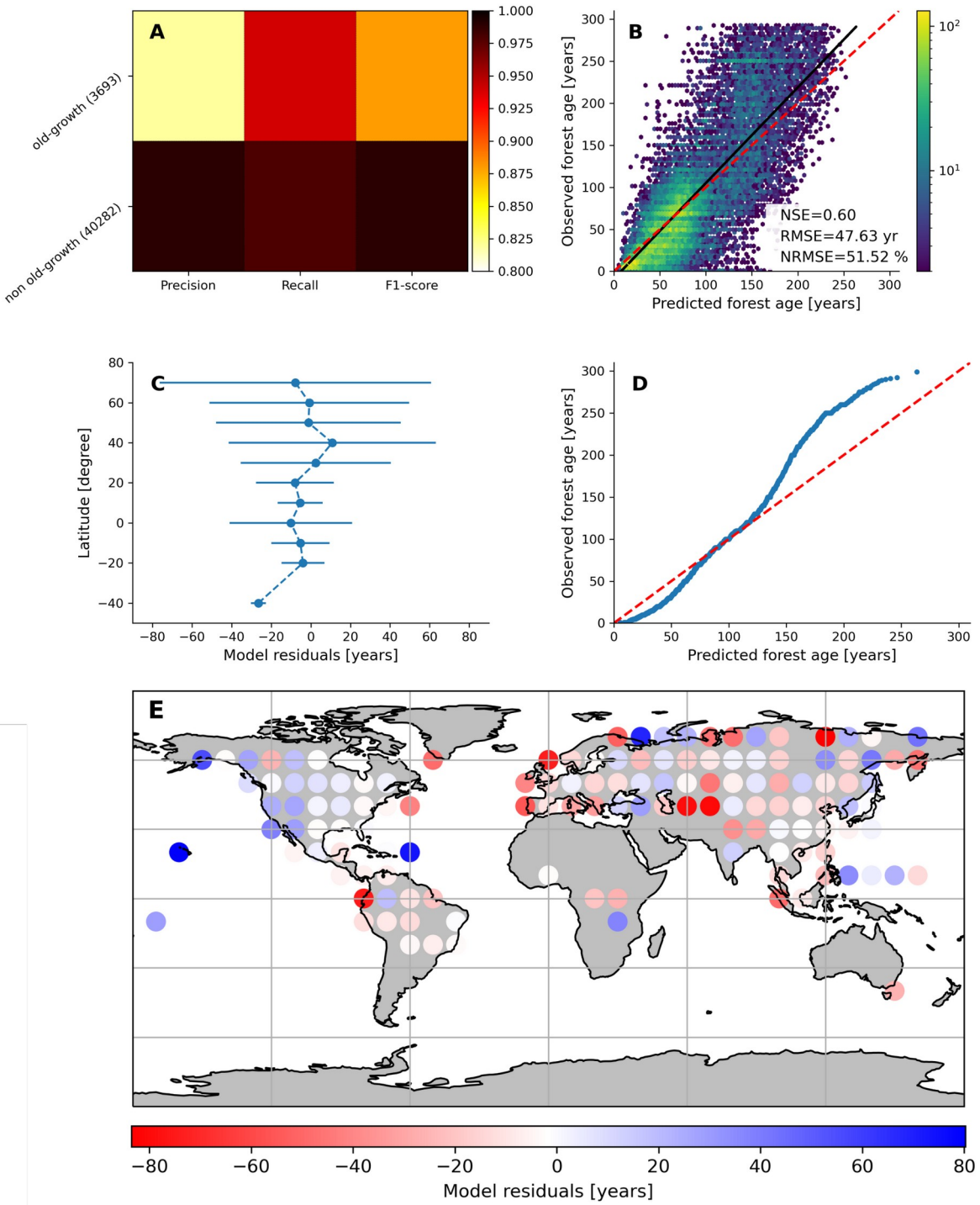

206 **Figure 3** Cross-validated results of the old-forests vs. non-old-forests classification (A) and comparison of predicted vs.
207 observed forest age estimates from the regression model (B). In C, the average model residuals ∓ standard deviation
208 within 10-degree latitudinal beans is shown. The quantile-quantile plot (D) is also shown.
209
210 We further investigated the variable importance of the selected variables and the functional relationships learned by the
211 RFregression model between forest age and these selected variables. For this, we computed the SHAP values for each
212 predictor to show how each predictor contributes, either positively or negatively, to the forest age estimates. First of all,
213 we observed that vapr was the most important variable, followed by agb and MeanTemperatureWettestQuarter (Fig. 4).
214 The importance of atmospheric water demand in explaining stand age variability could indicate how biomass is

associated with stand age across different climate regimes. More precisely, such observations could imply that high atmospheric water demand limits growth rates and maximum biomass, thereby indirectly controlling how biomass relates to age. In addition, high atmospheric water demand might influence fire frequency (Mueller et al., 2020) and indirectly control forest age distribution through the effect of fire on biomass. Biomass estimates contain information about the current state of the forest, integrating the cumulative effect of land-use change, management and disturbance history. Therefore, having biomass (i.e., agb) as an important variable in predicting forest age confirmed strong management and disturbance regime controls on the forest age distribution (Amiro et al., 2010).

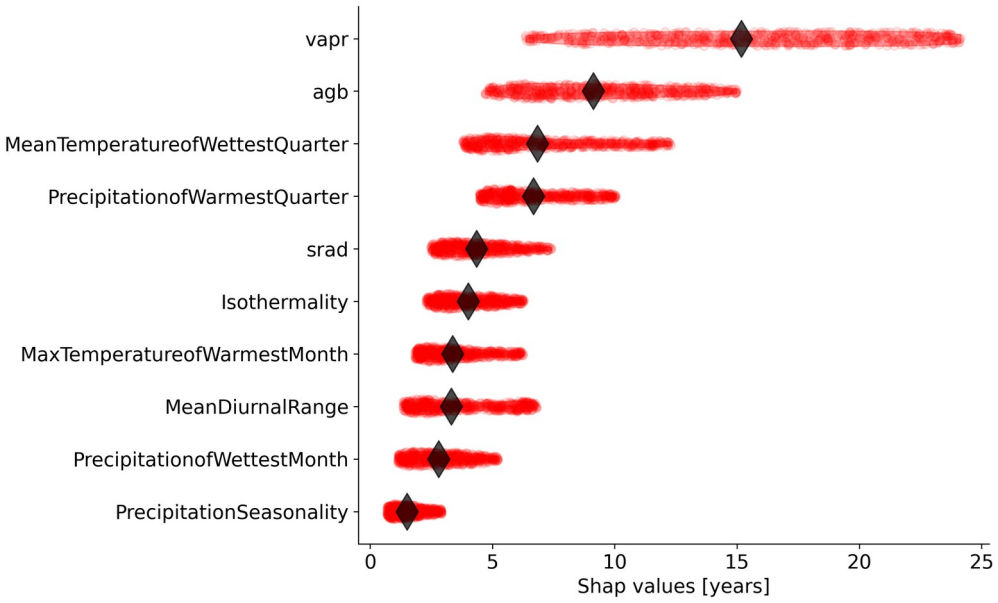

Figure 4 Relative importance of the independent variables selected by the feature selection algorithm in predicting forest age estimates in the RFregression model. Each dot represents the absolute SHAP value of one observation. The diamond represents the median value for each variable.

The emergent relationships revealed that an increase in AGB was associated with an increase in the forest age estimates (Fig. 5B). This relationship was expected as older trees have more carbon stored in the aboveground components than younger forests. The modelled forest age estimates appeared to be also relatively sensitive to the climatic conditions. For instance, we observed that climatic conditions with low water atmospheric demand (i.e., low vapr) (Fig. 5A) or conditions with high solar radiation (Fig. 5E) increased forest age. Similarly, we observed that forest age variability was also associated with air temperature conditions (Fig. 5C, F, G and H) and precipitation regimes (Fig. 5D and I).

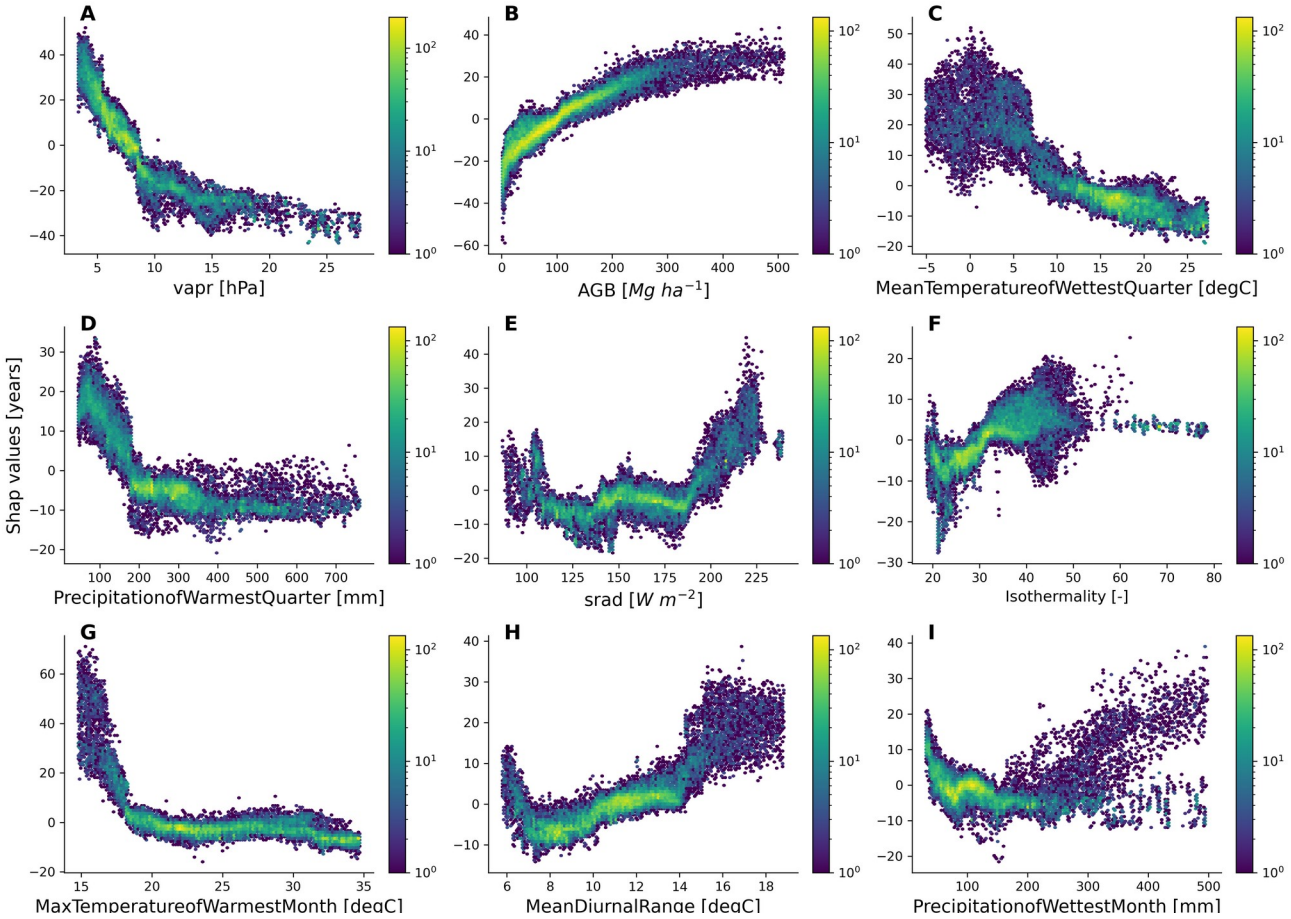

248 **Figure 5** Emergent relationships between the retrieved SHAP values and the independent variables selected by the
249 feature selection algorithm.
250
251 **3.2 Global forest age patterns and regional overview**

252 The MPI-BGC forest age product shows an extensive range of forest age across the globe (Fig. 6). We observed that the
253 most represented age class was the old-growth forests with around 1,1 billion hectares, while a limited fraction of very
254 young forest was observed (i.e., < 10 years old) (Fig. 6A). Not surprisingly, most of the old-growth/undisturbed forests
255 (+300 years old) can be found in the Amazon basin (Fig. 6B), the Congo basin (Fig. 6C) and part of the Indonesian
256 peninsula (Fig. 6H), where the minimal human disturbance occurred. A large area occupied by very young forests was
257 found in the Southeast part of China (Fig. 6H), probably due to afforestation/reforestation policies and natural
258 disturbances (Zhang et al., 2017). Similarly, young and intermediate forests were found in the African tropical dry
259 forests (i.e., Sahel and Miombo regions) (Fig. 6C), where the frequency of the fire regimes is very high, resulting in a
260 relatively young age-class structure (Werf et al., 2017). Large scale fires in the North American boreal region also
261 resulted in widespread patches of younger forests and a mosaic of stands of different ages since they last burned (Fig.
262 6G).
263 Furthermore, the unmanaged part of the North American boreal region near the ecotone, where fires are infrequent,
264 revealed older stands (Fig. 6G). Forests in British Columbia were generally old, although patches of younger forests
265 were probably in the early stages of disturbance recovery. European forests were in young/intermediate stages of forest
266 succession (Fig. 6E). The increased harvested forest area and considerable afforestation practices (Naudts et al., 2016)

probably explained a relatively young to intermediate forest demography and a mosaic of different age classes in the European region. The region of Siberia revealed a gradient of younger to older forests going from the South to the North part of the Siberian region (Fig. 6F). Such an observation could suggest different fire regimes between Southern and Northern Siberia (Shorohova et al., 2011) and confirm harvesting practices identified in Southern Siberia (Curtis et al., 2018). Finally, Australian forests were relatively young in the North part of the country while a mosaic of age class dominated the Southern part of Australia (Fig. 6D). The age patterns observed in the Northern part of Australia somehow correspond to the fact that forests are regrowing in this region (Pugh et al., 2019). However, it is essential to note that the few forest inventory plots in regions such as Australia (Fig. 1) could limit our certainty on the forest age estimates attributed by the statistical approaches due to, for instance, extrapolation issues. Another limitation is that we assumed forest homogeneity within a 1 km grid-cell, which would reduce the extremes of low and high biomass estimates in the gridded global products that the models have learned in the plot-level training data. This limitation might, for instance, explain the relative dearth of very young stands (1-10 years old) in the MPI-BGC global age product (Figs.6A).

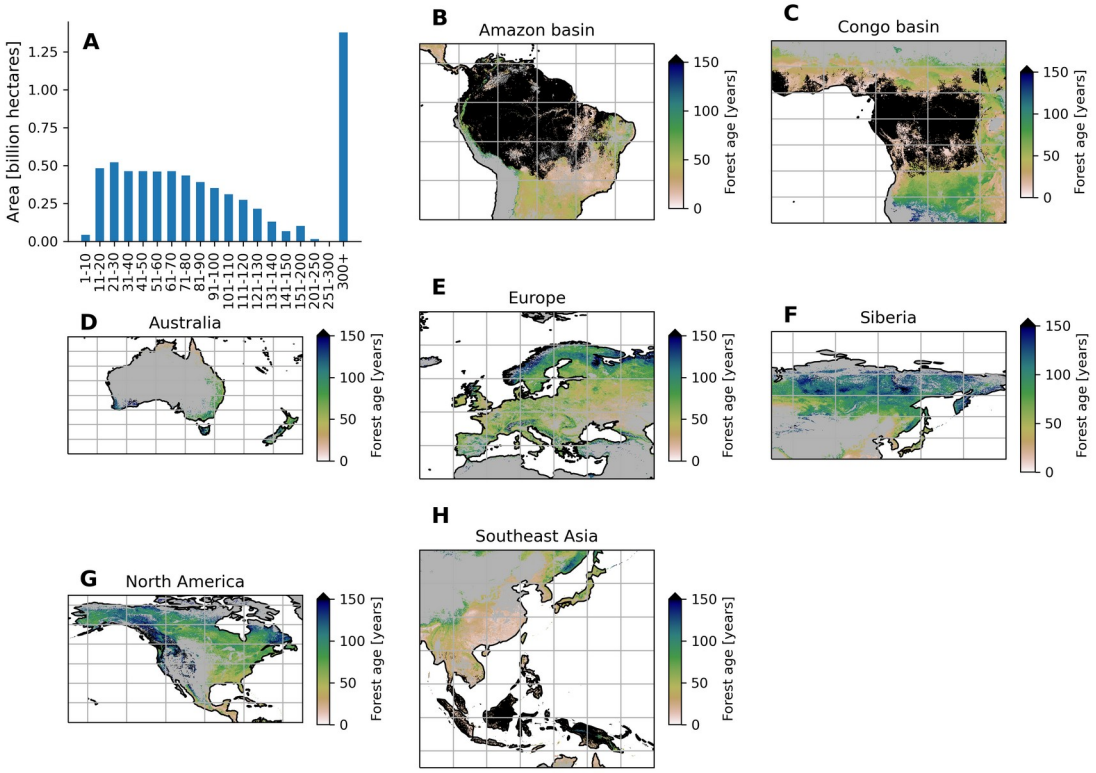

Figure 6 Total area of each age class globally (A) and close-up examples in the Amazon Basin (B), Congo Basin (C), Australia (D), Europe (E), Siberia (F), North America (G) and Southeast Asia (H). The forest age estimates in the close-up examples (B-H) range from 0 to 150 years old for better visualisation. The forest age map using a 10% tree cover threshold is shown.

3.3 Global forest age relationships with atmosphere, hydrosphere and vegetation conditions

We further investigated the distribution of the forest demography in the climate and vegetation spaces (Fig. 7). Generally, we observed that with warmer (i.e., air temperature) and drier (i.e., VPD) conditions, forests appeared to be younger with the expectation of old-growth tropical forests located in relatively warm climatic conditions (Fig. 7A).

Not surprisingly, we found that most of the old-growth tropical forests were located in regions with high productivity (i.e., high GPP and high biomass) (Fig. 7B), which coincides with our previous results investigating the structure of the statistical model showing that an increase in forest biomass was coupled with an increase in forest age (Fig. 5A). On the other hand, we observed that younger-intermediate forests were more productive than older forests outside the tropical old-growth forest envelope. More precisely, we found that forests being less productive will belong to an older age class for similar carbon stocks. Mature forests were found in cool temperatures and moderately low precipitation conditions (Fig. 7C), where rates of fast growth but slow decomposition generally drive forest dynamics. Younger stands were found in relatively warm conditions but a wide range of precipitation regimes (Fig. 7C). Finally, while a significant fraction of young forests were located in regions with low water availability and high water atmospheric demands, we also observed that above a certain threshold of water availability (i.e., > 0.4-0.5), the amount of water available for trees (i.e., IWA) was not directly associated with changes in forest age unlike VPD (Fig. 7D).

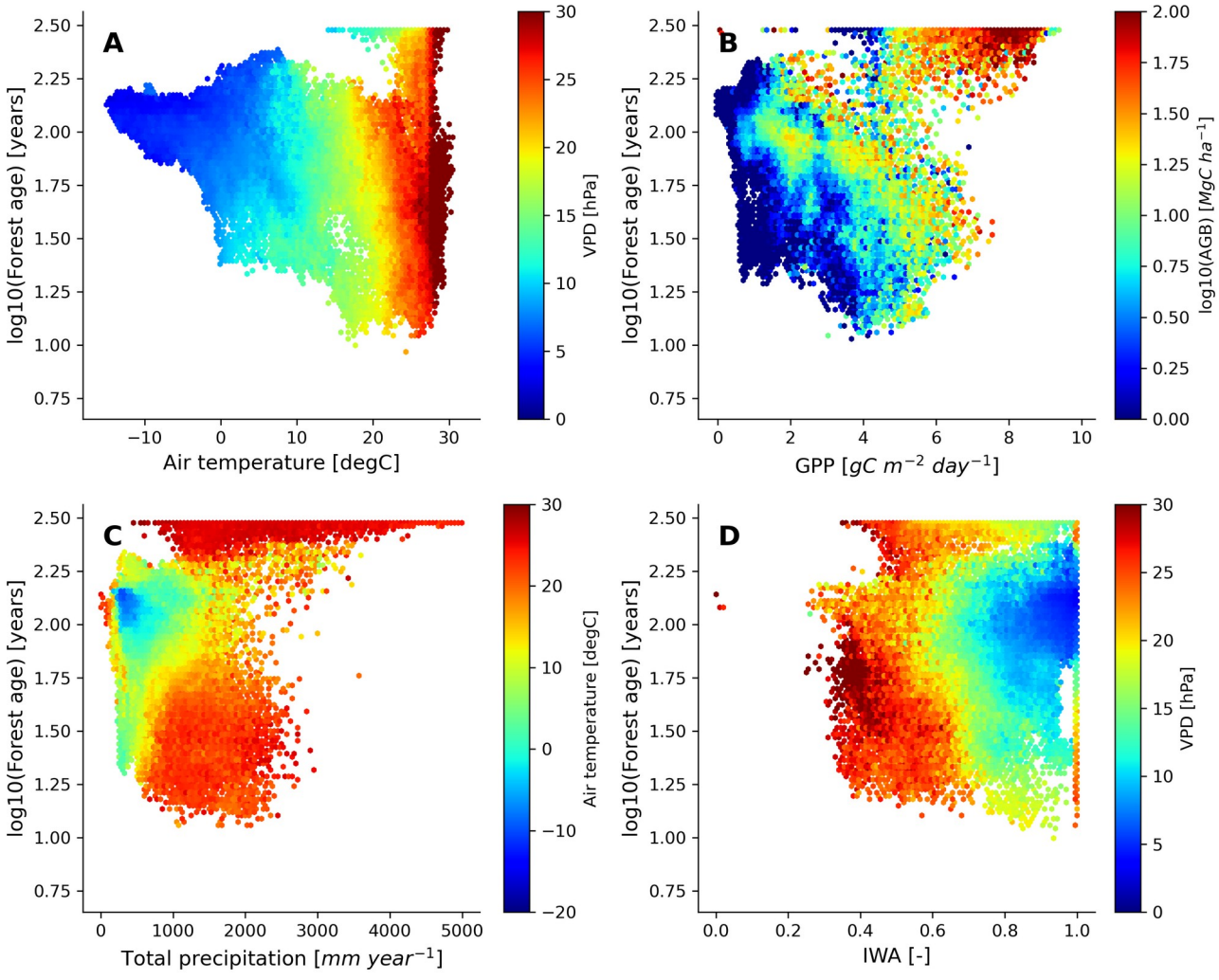

Figure 7 Forest age distribution in the climate, hydrological and productivity spaces defined by air temperature, vapour pressure deficit, total precipitation, soil water availability, GPP and above-ground biomass. The forest age map used here corresponds to a tree cover threshold of 10% aggregated to 0.25 degree using a weighted average of all non-NODATA contributing pixels. GPP is gross primary productivity derived from the FLUXCOM RS+meteo product

(Tramontana et al., 2016; Jung et al., 2011, 2020), and IWA is an index for soil water availability (Tramontana et al., 2016). The climatic variables were retrieved from the ERA5-reanalysis data (https://apps.ecmwf.int/datasets/licences/copernicus/). For all the climatic variables, we computed an annual mean for the year 2010.

3.4 Sensitivity analysis, uncertainties and comparison with previous products

We performed a sensitivity analysis using a series of AGB gridded products filtered with different tree cover thresholds to produce different global age products (see method section) (Fig. 8). This analysis showed that in South America, mainly the dry regions were sensitive to the tree cover threshold being applied, with forest age estimates being lower when no tree cover threshold was applied compared to a 30% tree cover correction (Fig. 8A). Similarly, we observed that the dry parts of the Congo basin depicted a sensitivity to the applied tree cover thresholds (Fig. 8B). In Europe, we observed widespread differences between the forest age estimated without a tree cover correction and with a tree cover correction (Fig. 8C). Generally, forest age estimates were higher when the 30% tree cover correction was applied. In Siberia (Fig. 8D), North America (Fig. 8E) and Southeast Asia (Fig. 8F), there were also large patches of forest where correcting the biomass maps with a tree cover threshold led to substantial differences in the age estimates. Overall, such observations were expected because of management practices or disturbance regimes, resulting in mosaic vegetation within a 1km grid cell. Such mosaic vegetation in regions such as the dry tropics (forest/grassland/shrubland), Europe (forests/croplands) and Northeast of the United States (forests/croplands) could explain the sensitivity of the forest age estimates to tree cover thresholds in these regions.

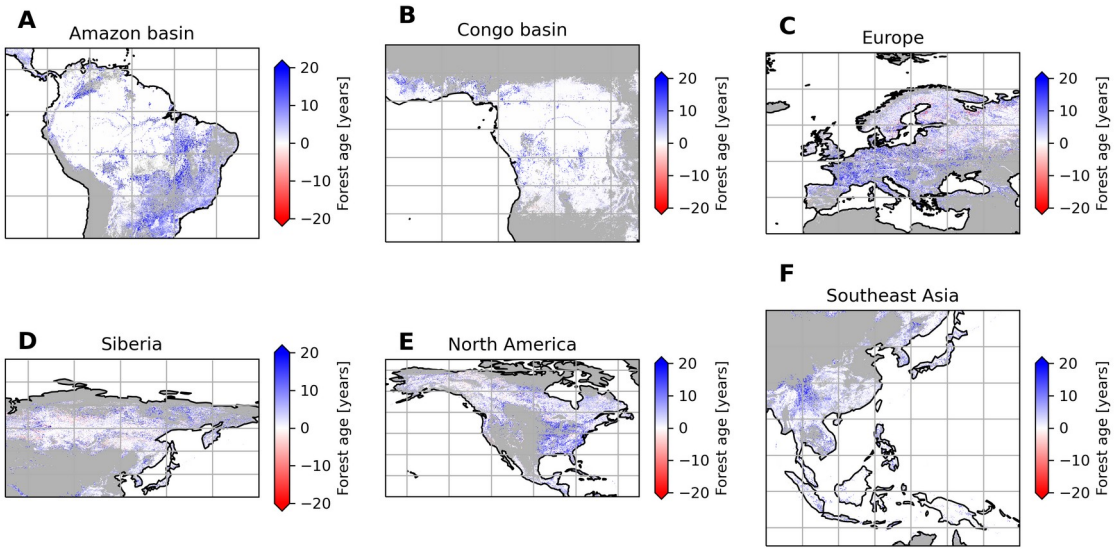

Figure 8 Sensitivity of the presented age product using 30% tree cover correction thresholds or no tree cover correction. The differences between the age estimates derived from a forest biomass product using a 30% tree cover correction and the age estimates derived from a forest biomass product not using a tree cover correction are shown. Blue colour means that the age estimates are higher with the 30% tree cover correction than without correction, while the red colour means that the age estimates are lower with the 30% tree cover correction than without correction.

Besides, we explored uncertainties associated with the two statistical models used for the upscaling procedure (Fig. S1, Fig. S2 and Fig. S3). First, we observed that the RFclassifier model had very high probabilities of classifying either a non-old-growth or an old-growth forest at pixel level as the fraction of the random forest ensemble to classify the two forest classes was generally close to one. (Fig. S1 and Fig. S2), suggesting relatively high confidence in the partitioning between old-growth and non-old-growth forests in the MPI-BGC forest age product. The regions at the edge of the Amazon and the Congo basins appeared to have the lowest confidence in classifying old-growth vs. non-old-growth forests (Fig. S1A, Fig. S1B and Fig. S2) with a probability close to 0.5. On the other hand, we observed relatively high probabilities for classifying non-old-growth forests in Europe (Fig. S1C), Siberia (Fig. S1D), North America (Fig. S1E) and Southeast Asia (Fig. S1F). We also provided uncertainties in predicting forest age estimates by retrieving the 25%, 50%, and 75% quantile predictions from the RFregressor model for computing the inter-quantile range (IQR, quantile 75% - quantile 25%) divided by the median (i.e., quantile 50%) of the forest age estimates (IQR/median) (Fig. S3). While in Europe (Fig. S3C), China (Fig. S3F) and the Eastern United States (Fig. S3E), the IQR/median estimates were relatively low, we observed high IQR/median estimates in Northern North American regions (Fig. S3E) as well as in large patches of Siberia (Fig. S3D) and the dry tropics (Fig. S3A and Fig. S3F).

We further compared the spatial patterns of the MPI-BGC forest age dataset with a series of independent regional and global forest age products (Chazdon et al., 2016; Pan et al., 2011; Poulter et al., 2019; Zhang et al., 2017) (Fig. 9, Fig. 10, and Fig. S5). In the Amazon basin, we found that the MPI-BGC forest age product depicted widespread higher forest age estimates (i.e., blue colour) than the Chazdon et al. (2016) dataset (Fig. 9A), resulting in a more extensive area of tropical old-growth forest in the MPI-BGC forest age product (Fig. 9B). On the other hand, we observed lower forest age estimates in the regions of Rio Grande Do Norte and Paraiba in the MPI-BGC forest age product (i.e., red colour). Such disagreement between the two products could be related not only to the different methods used to infer forest age (i.e., statistical method vs. age-AGB chronosequence approach for the MPI-BGC forest age and the Chazdon products, respectively) but also to the uncertainties of the RFclassifier for classifying old-growth vs. non-old-growth forests in this region (Fig. S1 and Fig. S2). Similarly, the presented product and the Pan dataset revealed widespread discrepancies in the North American region, particularly in the Western part of the United States and the North American boreal forests (Fig. 8E). More precisely, the Pan dataset had a higher fraction of young forest patches than the MPI-BGC forest age product (Fig. 9F). Methodological differences between the Pan and the MPI-BGC forest age datasets could explain such differences. While the Pan dataset integrates forest inventories, disturbance datasets, and land-use/land cover change data to retrieve forest age estimates in the Pan dataset, the MPI-BGC forest age product relied on forest inventory, climate data and statistical methods. Additionally, forest inventory plots used to derive the MPI-BGC forest age product were relatively sparse in Canada (Fig. 1), which might limit the statistical methods used for the MPI-BGC forest age product to predict realistic forest age estimates (i.e., extrapolation issues). Finally, the forest age estimates of China's MPI-BGC forest age product were consistent with the Zhang dataset (Fig. 9C). The area distribution across age classes of the two products appeared to have a relatively good agreement in China (Fig. 9D).

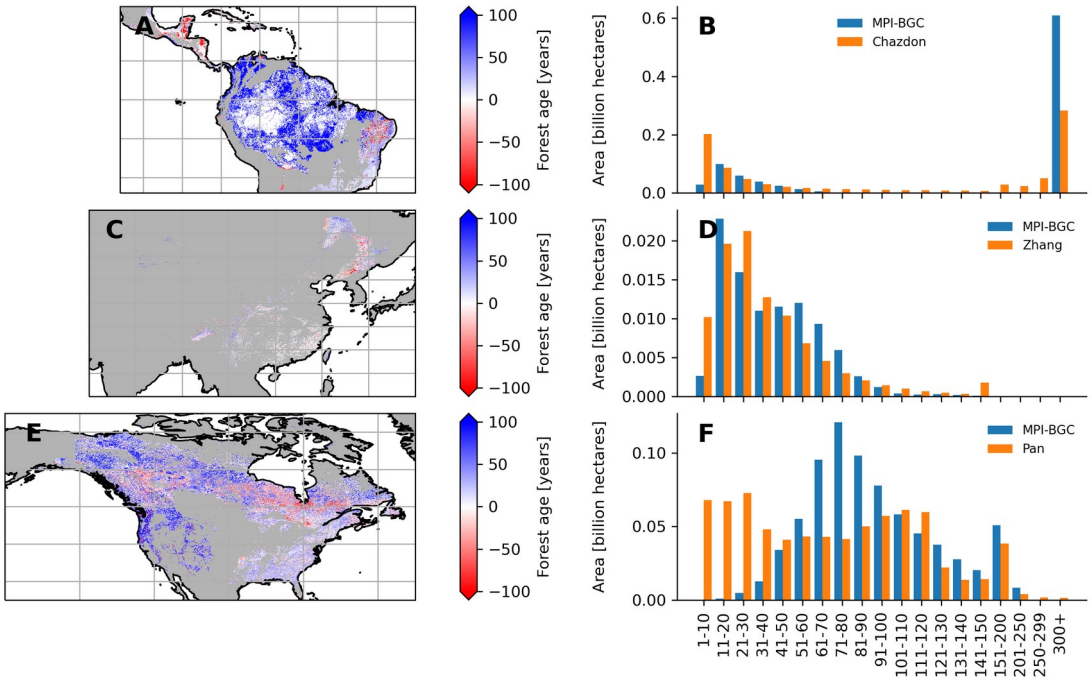

Figure 9 Comparison between the forest age dataset from this study and independent forest age dataset: Amazon basin (A and B), China (C and D) and North America (E and F). For a fair comparison with the independent age datasets, the MPI-BGC forest age map used here is the one without tree cover correction applied to the AGB dataset. Differences were computed using weighted age estimates from the fraction of the decadal age classes within each 0.5-degree grid cell resolution.

We also found significant and widespread discrepancies between the MPI-BGC forest age dataset and the global forest age dataset (GFAD) (Poulter et al., 2019) (Fig. 10). Overall, the GFAD product had higher fractions of very young and old forests (Fig. 10B and C). Because the GFAD used a different AGB product for the pan-tropical region and mainly relied on statistics from national forest inventories for the Northern hemisphere, widespread differences were expected between the GFAD and the MPI-BGC forest age maps. The MPI-BGC forest age dataset depicted older forests in the Western part of the United States (i.e., blue colour), while it showed younger forests across Europe than the GFAD product (Fig. 10A). Differences were also apparent in the dry tropics, where the GFAD product showed younger forests than the MPI-BGC forest age dataset, particularly in the Miombo regions. Such discrepancies could be explained either by the use of a biomass-age approach in this region or by integrating MODIS fire information in the GFAD forest age dataset. We adjusted the MPI-BGC forest age dataset with the forest age product inferred from the MCD45A1 MODerate-resolution Imaging Spectroradiometer (MODIS) fire product at 1 km resolution(Giglio et al., 2018; Poulter et al., 2019), which was used in the GFAD product. In this MODIS-age product, forest age was determined as the last time since a fire event occurred within a grid cell for 2000-2015, thereby assuming that the entire pixel was burned down. For instance, forest age within a 1 km grid cell was five years old if the last time a fire occurred within this grid cell was in 2010. The latter took precedence over the former dataset when adjusting the MPI-BGC forest age dataset with the MODIS-age product. As expected, we observed a higher fraction of younger forest in the adjusted MPI-BGC forest age dataset (Fig. S4B), particularly in regions relying on the biomass-age approach in the GFAD product (Fig. S4A and C). However, significant discrepancies between the two products remained when comparing the weighted average forest age estimates at the pixel level, particularly in European forests (Fig. S4A). Yet, we acknowledge that a

comparison between the GFAD and the MPI-BGC forest age maps has to be taken with caution when evaluating the MPI-BGC product as substantial methodological differences exist between the two products.

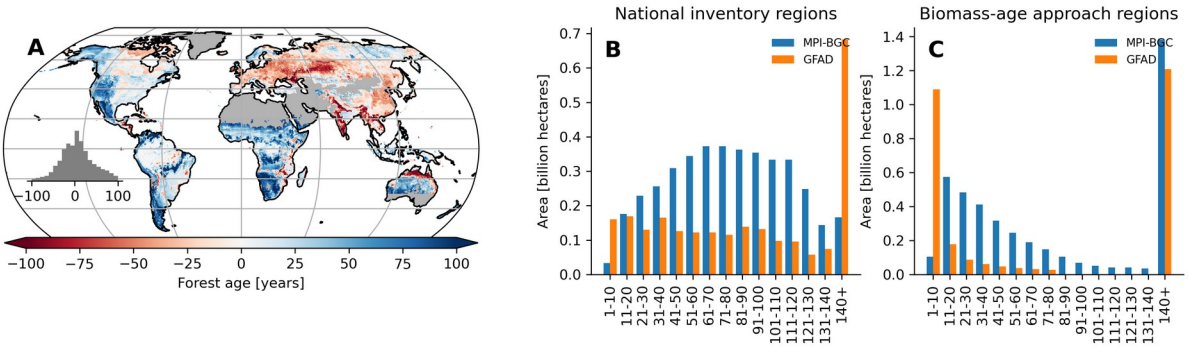

Figure 10 Difference map between the forest age estimates derived from the MPI-BGC and GFAD products (A). Areas per age class were also compared between the two products for regions relying on national inventories (B) and relying on biomass-age approach (C) in the GFAD product. Differences were computed using weighted age estimates from the fraction of the decadal age classes within each 0.5-degree grid cell resolution.

4 Data availability

The dataset of the different forest age products presented in this study can be downloaded from the Data Portal of the Max Planck Institute for Biogeochemistry at https://doi.org/10.17871/ForestAgeBGI.2021 (Besnard et al., 2021). For anonymous access during review, the data are available at https://nextcloud.bgc-jena.mpg.de/s/Xwt8AdkHkgL3TTc.

5 Conclusion

We presented a new forest age dataset derived from forest inventory, biomass, climate and remote sensing data. Generally, the statistical model used to create the gridded age datasets had a relatively good capacity to predict forest age estimates at plot level (precision of 0.81 and 0.99 for classifying old-growth and non-old-growth, respectively and NSE of 0.6 for predicting non-old-growth forests). At the same time, biases were observed, mainly when predicting older forests (i.e., > 150 years old). The functional relationships between biomass and forest age learned by the statistical models appeared to agree with forest age theory and the role of environmental/climate in modulating the relationship. The proposed gridded datasets allowed us to assess the global patterns of forest age and provided insights into regional forest demography. For instance, relatively young-intermediate forests were observed in Europe and China, where predominant management practices and afforestation/reforestation activities. We could also demonstrate that old forests are primarily represented in very wet, warm, and cold regions. However, comparing the MPI-BGC forest age product with independent forest age datasets revealed large discrepancies, suggesting high uncertainties in mapping forest demography globally. Overall, this forest age product provides a new source of information related to disturbance history and forest regrowth, which is crucial to better understanding the location of the forest carbon sinks and sources.

Author contributions

SB and NC designed the study. SB conducted analysis and wrote the paper under the direction of NC. SB, NC, SK, JG, and UW collected and harmonized the forest inventories datasets. BP, BH, JK, and AN provided data for the analysis. All authors contributed to the discussions and interpretation of the results and the writing of the paper.

Competing interests

The authors declare that they have no conflict of interest.

Acknowledgments

We would like to thank all the initiatives aiming to collect forest inventory plots. We thank the members of the Biogeochemical Integration Department at the Max Planck Institute for Biogeochemistry for providing feedback on the presented results. We acknowledge support by the European Union through the BIOMASCAT (https://eo4society.esa.int/projects/biomascat/) and VERIFY (776810) (https://cordis.europa.eu/project/id/776810) projects.

References

Álvarez-Dávila, E., Cayuela, L., González-Caro, S., Aldana, A. M., Stevenson, P. R., Phillips, O., Cogollo, Á., Peñuela, M. C., Hildebrand, P. von, Jiménez, E., Melo, O., Londoño-Vega, A. C., Mendoza, I., Velásquez, O., Fernández, F., Serna, M., Velázquez-Rua, C., Benítez, D., and Rey-Benayas, J. M.: Forest biomass density across large climate gradients in northern South America is related to water availability but not with temperature, PLOS ONE, 12, e0171072, https://doi.org/10.1371/journal.pone.0171072, 2017.

Amiro, B. D., Barr, A. G., Barr, J. G., Black, T. A., Bracho, R., Brown, M., Chen, J., Clark, K. L., Davis, K. J., Desai, A. R., Dore, S., Engel, V., Fuentes, J. D., Goldstein, A. H., Goulden, M. L., Kolb, T. E., Lavigne, M. B., Law, B. E., Margolis, H. A., Martin, T., McCaughey, J. H., Misson, L., Montes-Helu, M., Noormets, A., Randerson, J. T., Starr, G., and Xiao, J.: Ecosystem carbon dioxide fluxes after disturbance in forests of North America, 115, https://doi.org/10.1029/2010JG001390, 2010.

Anderson-Teixeira, K. J., Wang, M. M. H., McGarvey, J. C., and LeBauer, D. S.: Carbon dynamics of mature and regrowth tropical forests derived from a pantropical database (TropForC-db), 22, 1690–1709, https://doi.org/10.1111/gcb.13226, 2016.

Anderson-Teixeira, K. J., Wang, M. M. H., McGarvey, J. C., Herrmann, V., Tepley, A. J., Bond-Lamberty, B., and LeBauer, D. S.: ForC: a global database of forest carbon stocks and fluxes, Ecology, 99, 1507, https://doi.org/10.1002/ecy.2229, 2018.

Baker, T. R., Díaz, D. M. V., Moscoso, V. C., Navarro, G., Monteagudo, A., Pinto, R., Cangani, K., Fyllas, N. M., Gonzalez, G. L., Laurance, W. F., Lewis, S. L., Lloyd, J., Steege, H. ter, Terborgh, J. W., and Phillips, O. L.: Consistent, small effects of treefall disturbances on the composition and diversity of four Amazonian forests, 104, 497–506, https://doi.org/10.1111/1365-2745.12529, 2016.

Bar-On, Y. M., Phillips, R., and Milo, R.: The biomass distribution on Earth, 115, 6506–6511, https://doi.org/10.1073/pnas.1711842115, 2018.

Besnard, S., Carvalhais, N., Arain, M. A., Black, A., Bruin, S. de, Buchmann, N., Cescatti, A., Chen, J., Clevers, J. G. P. W., Desai, A. R., Gough, C. M., Havrankova, K., Herold, M., Hörtnagl, L., Jung, M., Knohl, A., Kruijt, B., Krupkova, L., Law, B. E., Lindroth, A., Noormets, A., Roupsard, O., Steinbrecher, R., Varlagin, A., Vincke, C., and Reichstein, M.: Quantifying the effect of forest age in annual net forest carbon balance, Environ. Res. Lett., 13, 124018, https://doi.org/10.1088/1748-9326/aaeaeb, 2018.

Birdsey, R., Pregitzer, K., and Lucier, A.: Forest carbon management in the United States: 1600-2100, J. Environ. Qual., 35, 1461–1469, https://doi.org/10.2134/jeq2005.0162, 2006.

Bowman, D. M. J. S., Balch, J. K., Artaxo, P., Bond, W. J., Carlson, J. M., Cochrane, M. A., D'Antonio, C. M., DeFries, R. S., Doyle, J. C., Harrison, S. P., Johnston, F. H., Keeley, J. E., Krawchuk, M. A., Kull, C. A., Marston, J. B., Moritz, M. A., Prentice, I. C., Roos, C. I., Scott, A. C., Swetnam, T. W., Werf, G. R. van der, and Pyne, S. J.: Fire in the Earth System, 324, 481–484, https://doi.org/10.1126/science.1163886, 2009.

Buitenwerf, R., Sandel, B., Normand, S., Mimet, A., and Svenning, J.-C.: Land surface greening suggests vigorous woody regrowth throughout European semi-natural vegetation, Global Change Biology, 24, 5789–5801, https://doi.org/10.1111/gcb.14451, 2018.

Chazdon, R. L., Broadbent, E. N., Rozendaal, D. M. A., Bongers, F., Zambrano, A. M. A., Aide, T. M., Balvanera, P., Becknell, J. M., Boukili, V., Brancalion, P. H. S., Craven, D., Almeida-Cortez, J. S., Cabral, G. A. L., Jong, B. de, Denslow, J. S., Dent, D. H., DeWalt, S. J., Dupuy, J. M., Durán, S. M., Espírito-Santo, M. M., Fandino, M. C., César, R. G., Hall, J. S., Hernández-Stefanoni, J. L., Jakovac, C. C., Junqueira, A. B., Kennard, D., Letcher, S. G., Lohbeck, M., Martínez-Ramos, M., Massoca, P., Meave, J. A., Mesquita, R., Mora, F., Muñoz, R., Muscarella, R., Nunes, Y. R. F., Ochoa-Gaona, S., Orihuela-Belmonte, E., Peña-Claros, M., Pérez-García, E. A., Piotto, D., Powers, J. S., Rodríguez-Velazquez, J., Romero-Pérez, I. E., Ruíz, J., Saldarriaga, J. G., Sanchez-Azofeifa, A., Schwartz, N. B., Steininger, M. K., Swenson, N. G., Uriarte, M., Breugel, M. van, Wal, H. van der, Veloso, M. D. M., Vester, H., Vieira, I. C. G., Bentos, T. V., Williamson, G. B., and Poorter, L.: Carbon sequestration potential of second-growth forest regeneration in the Latin American tropics, 2, e1501639, https://doi.org/10.1126/sciadv.1501639, 2016.

Ciais, P., Dolman, A. J., Bombelli, A., Duren, R., Peregon, A., Rayner, P. J., Miller, C., Gobron, N., Kinderman, G., Marland, G., Gruber, N., Chevallier, F., Andres, R. J., Balsamo, G., Bopp, L., Bréon, F.-M., Broquet, G., Dargaville, R., Battin, T. J., Borges, A., Bovensmann, H., Buchwitz, M., Butler, J., Canadell, J. G., Cook, R. B., DeFries, R., Engelen, R., Gurney, K. R., Heinze, C., Heimann, M., Held, A., Henry, M., Law, B., Luyssaert, S., Miller, J., Moriyama, T., Moulin, C., Myneni, R. B., Nussli, C., Obersteiner, M., Ojima, D., Pan, Y., Paris, J.-D., Piao, S. L., Poulter, B., Plummer, S., Quegan, S., Raymond, P., Reichstein, M., Rivier, L., Sabine, C., Schimel, D., Tarasova, O., Valentini, R., Wang, R., van der Werf, G., Wickland, D., Williams, M., and Zehner, C.: Current systematic carbon-cycle observations and the need for implementing a policy-relevant carbon observing system, 11, 3547–3602, https://doi.org/10.5194/bg-11-3547-2014, 2014.

Cook-Patton, S. C., Leavitt, S. M., Gibbs, D., Harris, N. L., Lister, K., Anderson-Teixeira, K. J., Briggs, R. D., Chazdon, R. L., Crowther, T. W., Ellis, P. W., Griscom, H. P., Herrmann, V., Holl, K. D., Houghton, R. A., Larrosa, C., Lomax, G., Lucas, R., Madsen, P., Malhi, Y., Paquette, A., Parker, J. D., Paul, K., Routh, D., Roxburgh, S., Saatchi, S., van den Hoogen, J., Walker, W. S., Wheeler, C. E., Wood, S. A., Xu, L., and Griscom, B. W.: Mapping carbon accumulation potential from global natural forest regrowth, 585, 545–550, https://doi.org/10.1038/s41586-020-2686-x, 2020.

Curtis, P. G., Slay, C. M., Harris, N. L., Tyukavina, A., and Hansen, M. C.: Classifying drivers of global forest loss, 361, 1108–1111, https://doi.org/10.1126/science.aau3445, 2018.

Fick, S. E. and Hijmans, R. J.: WorldClim 2: new 1-km spatial resolution climate surfaces for global land areas, 37, 4302–4315, https://doi.org/10.1002/joc.5086, 2017.

Giglio, L., Boschetti, L., Roy, D. P., Humber, M. L., and Justice, C. O.: The Collection 6 MODIS burned area mapping algorithm and product, Remote Sensing of Environment, 217, 72–85, https://doi.org/10.1016/j.rse.2018.08.005, 2018.

Guyon, I., Weston, J., Barnhill, S., and Vapnik, V.: Gene Selection for Cancer Classification using Support Vector Machines, Machine Learning, 46, 389–422, https://doi.org/10.1023/A:1012487302797, 2002.

Hansen, M. C., Potapov, P. V., Moore, R., Hancher, M., Turubanova, S. A., Tyukavina, A., Thau, D., Stehman, S. V., Goetz, S. J., Loveland, T. R., Kommareddy, A., Egorov, A., Chini, L., Justice, C. O., and Townshend, J. R. G.: High-Resolution Global Maps of 21st-Century Forest Cover Change, 342, 850–853, https://doi.org/10.1126/science.1244693, 2013.

Huang, C., Goward, S. N., Masek, J. G., Thomas, N., Zhu, Z., and Vogelmann, J. E.: An automated approach for reconstructing recent forest disturbance history using dense Landsat time series stacks, 114, 183–198, https://doi.org/10.1016/j.rse.2009.08.017, 2010.

Irvine, J., Law, B. E., and Kurpius, M. R.: Coupling of canopy gas exchange with root and rhizosphere respiration in a semi-arid forest, Biogeochemistry, 73, 271–282, https://doi.org/10.1007/s10533-004-2564-x, 2005.

Johnson, D. W. and Curtis, P. S.: Effects of forest management on soil C and N storage: meta analysis, Forest Ecology and Management, 140, 227–238, https://doi.org/10.1016/S0378-1127(00)00282-6, 2001.

Johnson, M. O., Galbraith, D., Gloor, M., Deurwaerder, H. D., Guimberteau, M., Rammig, A., Thonicke, K., Verbeeck, H., Randow, C. von, Monteagudo, A., Phillips, O. L., Brienen, R. J. W., Feldpausch, T. R., Gonzalez, G. L., Fauset, S., Quesada, C. A., Christoffersen, B., Ciais, P., Sampaio, G., Kruijt, B., Meir, P., Moorcroft, P., Zhang, K., Alvarez-Davila, E., Oliveira, A. A. de, Amaral, I., Andrade, A., Aragao, L. E. O. C., Araujo-Murakami, A., Arets, E. J. M. M., Arroyo, L., Aymard, G. A., Baraloto, C., Barroso, J., Bonal, D., Boot, R., Camargo, J., Chave, J., Cogollo, A., Valverde, F. C., Costa, A. C. L. da, Fiore, A. D., Ferreira, L., Higuchi, N., Honorio, E. N., Killeen, T. J., Laurance, S. G., Laurance, W. F., Licona, J., Lovejoy, T., Malhi, Y., Marimon, B., Marimon, B. H., Matos, D. C. L., Mendoza, C., Neill, D. A., Pardo, G., Peña-Claros, M., Pitman, N. C. A., Poorter, L., Prieto, A., Ramirez-Angulo, H., Roopsind, A., Rudas, A., Salomao, R. P., Silveira, M., Stropp, J., Steege, H. ter, Terborgh, J., Thomas, R., Toledo, M., Torres-Lezama, A., Heijden, G. M. F. van der, Vasquez, R., Vieira, I. C. G., Vilanova, E., Vos, V. A., and Baker, T. R.: Variation in stem mortality rates determines patterns of above-ground biomass in Amazonian forests: implications for dynamic global vegetation models, 22, 3996–4013, https://doi.org/10.1111/gcb.13315, 2016.

Jung, M., Reichstein, M., Margolis, H. A., Cescatti, A., Richardson, A. D., Arain, M. A., Arneth, A., Bernhofer, C., Bonal, D., Chen, J., Gianelle, D., Gobron, N., Kiely, G., Kutsch, W., Lasslop, G., Law, B. E., Lindroth, A., Merbold, L., Montagnani, L., Moors, E. J., Papale, D., Sottocornola, M., Vaccari, F., and Williams, C.: Global patterns of land-atmosphere fluxes of carbon dioxide, latent heat, and sensible heat derived from eddy covariance, satellite, and meteorological observations, Journal of Geophysical Research: Biogeosciences, 116, https://doi.org/10.1029/2010JG001566, 2011.

Jung, M., Schwalm, C., Migliavacca, M., Walther, S., Camps-Valls, G., Koirala, S., Anthoni, P., Besnard, S., Bodesheim, P., Carvalhais, N., Chevallier, F., Gans, F., Goll, D. S., Haverd, V., Köhler, P., Ichii, K., Jain, A. K., Liu, J., Lombardozzi, D., Nabel, J. E. M. S., Nelson, J. A., O'Sullivan, M., Pallandt, M., Papale, D., Peters, W., Pongratz, J., Rödenbeck, C., Sitch, S., Tramontana, G., Walker, A., Weber, U., and Reichstein, M.: Scaling carbon fluxes from eddy covariance sites to globe: synthesis and evaluation of the FLUXCOM approach, 17, 1343–1365, https://doi.org/10.5194/bg-17-1343-2020, 2020.

Kennedy, R. E., Yang, Z., and Cohen, W. B.: Detecting trends in forest disturbance and recovery using yearly Landsat time series: 1. LandTrendr — Temporal segmentation algorithms, Remote Sensing of Environment, 114, 2897–2910, https://doi.org/10.1016/j.rse.2010.07.008, 2010.

Lewis, S. L., Sonké, B., Sunderland, T., Begne, S. K., Lopez-Gonzalez, G., van der Heijden, G. M. F., Phillips, O. L., Affum-Baffoe, K., Baker, T. R., Banin, L., Bastin, J.-F., Beeckman, H., Boeckx, P., Bogaert, J., De Cannière, C., Chezeaux, E., Clark, C. J., Collins, M., Djagbletey, G., Djuikouo, M. N. K., Droissart, V., Doucet, J.-L., Ewango, C. E. N., Fauset, S., Feldpausch, T. R., Foli, E. G., Gillet, J.-F., Hamilton, A. C., Harris, D. J., Hart, T. B., de Haulleville, T., Hladik, A., Hufkens, K., Huygens, D., Jeanmart, P., Jeffery, K. J., Kearsley, E., Leal, M. E., Lloyd, J., Lovett, J. C., Makana, J.-R., Malhi, Y., Marshall, A. R., Ojo, L., Peh, K. S.-H., Pickavance, G., Poulsen, J. R., Reitsma, J. M., Sheil, D., Simo, M., Steppe, K., Taedoumg, H. E., Talbot, J., Taplin, J. R. D., Taylor, D., Thomas, S. C., Toirambe, B., Verbeeck, H., Vleminckx, J., White, L. J. T., Willcock, S., Woell, H., and Zemagho, L.: Above-ground biomass and structure of 260 African tropical forests, 368, 20120295, https://doi.org/10.1098/rstb.2012.0295, 2013.

Liu, S., Bond-Lamberty, B., Hicke, J. A., Vargas, R., Zhao, S., Chen, J., Edburg, S. L., Hu, Y., Liu, J., McGuire, A. D., Xiao, J., Keane, R., Yuan, W., Tang, J., Luo, Y., Potter, C., and Oeding, J.: Simulating the impacts of disturbances on forest carbon cycling in North America: Processes, data, models, and challenges, 116, https://doi.org/10.1029/2010JG001585, 2011.

Lundberg, S. and Lee, S.-I.: A Unified Approach to Interpreting Model Predictions, 2017.

Lundberg, S. M., Erion, G. G., and Lee, S.-I.: Consistent Individualized Feature Attribution for Tree Ensembles, 2019.

Mitchard, E. T. A., Feldpausch, T. R., Brienen, R. J. W., Lopez-Gonzalez, G., Monteagudo, A., Baker, T. R., Lewis, S. L., Lloyd, J., Quesada, C. A., Gloor, M., Steege, H. ter, Meir, P., Alvarez, E., Araujo-Murakami, A., Aragão, L. E. O. C., Arroyo, L., Aymard, G., Banki, O., Bonal, D., Brown, S., Brown, F. I., Cerón, C. E., Moscoso, V. C., Chave, J., Comiskey, J. A., Cornejo, F., Medina, M. C., Costa, L. D., Costa, F. R. C., Fiore, A. D., Domingues, T. F., Erwin, T. L., Frederickson, T., Higuchi, N., Coronado, E. N. H., Killeen, T. J., Laurance, W. F., Levis, C., Magnusson, W. E., Marimon, B. S., Junior, B. H. M., Polo, I. M., Mishra, P., Nascimento, M. T., Neill, D., Vargas, M. P. N., Palacios, W. A., Parada, A., Molina, G. P., Peña-Claros, M., Pitman, N., Peres, C. A., Poorter, L., Prieto, A., Ramirez-Angulo, H., Correa, Z. R., Roopsind, A., Roucoux, K. H., Rudas, A., Salomão, R. P., Schietti, J., Silveira, M., Souza, P. F. de, Steininger, M. K., Stropp, J., Terborgh, J., Thomas, R., Toledo, M., Torres-Lezama, A., Andel, T. R. van, Heijden, G. M. F. van der, Vieira, I. C. G., Vieira, S., Vilanova-Torre, E., Vos, V. A., Wang, O., Zartman, C. E., Malhi, Y., and Phillips, O. L.: Markedly divergent estimates of Amazon forest carbon density from ground plots and satellites, 23, 935–946, https://doi.org/10.1111/geb.12168, 2014.

Moore, D. J. P., Trahan, N. A., Wilkes, P., Quaife, T., Stephens, B. B., Elder, K., Desai, A. R., Negron, J., and Monson, R. K.: Persistent reduced ecosystem respiration after insect disturbance in high elevation forests, 16, 731–737, https://doi.org/10.1111/ele.12097, 2013.

Mueller, S. E., Thode, A. E., Margolis, E. Q., Yocom, L. L., Young, J. D., and Iniguez, J. M.: Climate relationships with increasing wildfire in the southwestern US from 1984 to 2015, Forest Ecology and Management, 460, 117861, https://doi.org/10.1016/j.foreco.2019.117861, 2020.

Naudts, K., Chen, Y., McGrath, M. J., Ryder, J., Valade, A., Otto, J., and Luyssaert, S.: Europe's forest management did not mitigate climate warming, 351, 597–600, https://doi.org/10.1126/science.aad7270, 2016.

N'Guessan, A. E., N'dja, J. K., Yao, O. N., Amani, B. H. K., Gouli, R. G. Z., Piponiot, C., Zo-Bi, I. C., and Hérault, B.: Drivers of biomass recovery in a secondary forested landscape of West Africa, Forest Ecology and Management, 433, 325–331, https://doi.org/10.1016/j.foreco.2018.11.021, 2019.

Odum, E. P.: The Strategy of Ecosystem Development, 164, 262–270, https://doi.org/10.1126/science.164.3877.262, 1969.

Pan, Y., Chen, J. M., Birdsey, R., McCullough, K., He, L., and Deng, F.: Age structure and disturbance legacy of North American forests, 8, 715–732, https://doi.org/10.5194/bg-8-715-2011, 2011.

Piponiot, C., Derroire, G., Descroix, L., Mazzei, L., Rutishauser, E., Sist, P., and Hérault, B.: Assessing timber volume recovery after disturbance in tropical forests – A new modelling framework, Ecological Modelling, 384, 353–369, https://doi.org/10.1016/j.ecolmodel.2018.05.023, 2018.

Ploton, P., Mortier, F., Réjou-Méchain, M., Barbier, N., Picard, N., Rossi, V., Dormann, C., Cornu, G., Viennois, G., Bayol, N., Lyapustin, A., Gourlet-Fleury, S., and Pélissier, R.: Spatial validation reveals poor predictive performance of large-scale ecological mapping models, Nat Commun, 11, 4540, https://doi.org/10.1038/s41467-020-18321-y, 2020.

Poorter, L., Bongers, F., Aide, T. M., Almeyda Zambrano, A. M., Balvanera, P., Becknell, J. M., Boukili, V., Brancalion, P. H. S., Broadbent, E. N., Chazdon, R. L., Craven, D., de Almeida-Cortez, J. S., Cabral, G. A. L., de Jong, B. H. J., Denslow, J. S., Dent, D. H., DeWalt, S. J., Dupuy, J. M., Durán, S. M., Espírito-Santo, M. M., Fandino, M. C., César, R. G., Hall, J. S., Hernandez-Stefanoni, J. L., Jakovac, C. C., Junqueira, A. B., Kennard, D., Letcher, S. G., Licona, J.-C., Lohbeck, M., Marín-Spiotta, E., Martínez-Ramos, M., Massoca, P., Meave, J. A., Mesquita, R., Mora, F., Muñoz, R., Muscarella, R., Nunes, Y. R. F., Ochoa-Gaona, S., de Oliveira, A. A., Orihuela-Belmonte, E., Peña-Claros, M., Pérez-García, E. A., Piotto, D., Powers, J. S., Rodríguez-Velázquez, J., Romero-Pérez, I. E., Ruíz, J., Saldarriaga, J. G., Sanchez-Azofeifa, A., Schwartz, N. B., Steininger, M. K., Swenson, N. G., Toledo, M., Uriarte, M., van Breugel, M., van der Wal, H., Veloso, M. D. M., Vester, H. F. M., Vicentini, A., Vieira, I. C. G., Bentos, T. V., Williamson, G. B., and Rozendaal, D. M. A.: Biomass resilience of Neotropical secondary forests, 530, 211–214, https://doi.org/10.1038/nature16512, 2016.

Poulter, B., Aragão, L., Andela, N., Bellassen, V., Ciais, P., Kato, T., Lin, X., Nachin, B., Luyssaert, S., Pederson, N., Peylin, P., Piao, S., Pugh, T., Saatchi, S., Schepaschenko, D., Schelhaas, M., and Shivdenko, A.: The global forest age dataset and its uncertainties (GFADv1.1), https://doi.org/10.1594/PANGAEA.897392, 2019.

Pugh, T. A. M., Lindeskog, M., Smith, B., Poulter, B., Arneth, A., Haverd, V., and Calle, L.: Role of forest regrowth in global carbon sink dynamics, PNAS, 201810512, https://doi.org/10.1073/pnas.1810512116, 2019.

Santoro, M., Cartus, O., Carvalhais, N., Rozendaal, D. M. A., Avitabile, V., Araza, A., de Bruin, S., Herold, M., Quegan, S., Rodríguez-Veiga, P., Balzter, H., Carreiras, J., Schepaschenko, D., Korets, M., Shimada, M., Itoh, T., Moreno Martínez, Á., Cavlovic, J., Cazzolla Gatti, R., da Conceição Bispo, P., Dewnath, N., Labrière, N., Liang, J., Lindsell, J., Mitchard, E. T. A., Morel, A., Pacheco Pascagaza, A. M., Ryan, C. M., Slik, F., Vaglio Laurin, G., Verbeeck, H., Wijaya, A., and Willcock, S.: The global forest above-ground biomass pool for 2010 estimated from high-resolution satellite observations, 13, 3927–3950, https://doi.org/10.5194/essd-13-3927-2021, 2021.

Schepaschenko, D., Shvidenko, A., Usoltsev, V., Lakyda, P., Luo, Y., Vasylyshyn, R., Lakyda, I., Myklush, Y., See, L., McCallum, I., Fritz, S., Kraxner, F., and Obersteiner, M.: A dataset of forest biomass structure for Eurasia, 4, 170070, https://doi.org/10.1038/sdata.2017.70, 2017.

Shorohova, E., Kneeshaw, D., Kuuluvainen, T., and Gauthier, S.: VARIABILITY AND DYNAMICS OF OLD-GROWTH FORESTS IN THE CIRCUMBOREAL ZONE: IMPLICATIONS FOR CONSERVATION, RESTORATION AND MANAGEMENT, https://doi.org/10.14214/SF.72, 2011.

Somogyi, Z., Teobaldelli, M., Federici, S., Matteucci, G., Pagliari, V., Grassi, G., and Seufert, G.: Allometric biomass and carbon factors database, 1, 107, https://doi.org/10.3832/ifor0463-0010107, 2008.

Sulla-Menashe, D., Woodcock, C. E., and Friedl, M. A.: Canadian boreal forest greening and browning trends: an analysis of biogeographic patterns and the relative roles of disturbance versus climate drivers, Environ. Res. Lett., 13, 014007, https://doi.org/10.1088/1748-9326/aa9b88, 2018.

Sullivan, M. J. P., Talbot, J., Lewis, S. L., Phillips, O. L., Qie, L., Begne, S. K., Chave, J., Cuni-Sanchez, A., Hubau, W., Lopez-Gonzalez, G., Miles, L., Monteagudo-Mendoza, A., Sonké, B., Sunderland, T., ter Steege, H., White, L. J. T., Affum-Baffoe, K., Aiba, S., de Almeida, E. C., de Oliveira, E. A., Alvarez-Loayza, P., Dávila, E. Á., Andrade, A., Aragão, L. E. O. C., Ashton, P., C, G. A. A., Baker, T. R., Balinga, M., Banin, L. F., Baraloto, C., Bastin, J.-F., Berry, N., Bogaert, J., Bonal, D., Bongers, F., Brienen, R., Camargo, J. L. C., Cerón, C., Moscoso, V. C., Chezeaux, E., Clark, C. J., Pacheco, Á. C., Comiskey, J. A., Valverde, F. C., Coronado, E. N. H., Dargie, G., Davies, S. J., De Canniere, C., K, M. N. D., Doucet, J.-L., Erwin, T. L., Espejo, J. S., Ewango, C. E. N., Fauset, S., Feldpausch, T. R., Herrera, R., Gilpin, M., Gloor, E., Hall, J. S., Harris, D. J., Hart, T. B., Kartawinata, K., Kho, L. K., Kitayama, K., Laurance, S. G. W., Laurance, W. F., Leal, M. E., Lovejoy, T., Lovett, J. C., Lukasu, F. M., Makana, J.-R., Malhi, Y., Maracahipes, L., Marimon, B. S., Junior, B. H. M., Marshall, A. R., Morandi, P. S., Mukendi, J. T., Mukinzi, J., Nilus, R., Vargas, P. N., Camacho, N. C. P., Pardo, G., Peña-Claros, M., Pétronelli, P., Pickavance, G. C., Poulsen, A. D., Poulsen, J. R., Primack, R. B., Priyadi, H., Quesada, C. A., Reitsma, J., Réjou-Méchain, M., Restrepo, Z., Rutishauser, E., Salim, K. A., Salomão, R. P., Samsoedin, I., Sheil, D., et al.: Diversity and carbon storage across the tropical forest biome, 7, 39102, https://doi.org/10.1038/srep39102, 2017.

Tramontana, G., Jung, M., Schwalm, C. R., Ichii, K., Camps-Valls, G., Ráduly, B., Reichstein, M., Arain, M. A., Cescatti, A., Kiely, G., Merbold, L., Serrano-Ortiz, P., Sickert, S., Wolf, S., and Papale, D.: Predicting carbon dioxide and energy fluxes across global FLUXNET sites with regression algorithms, 13, 4291–4313, https://doi.org/10.5194/bg-13-4291-2016, 2016.

Werf, G. R. van der, Randerson, J. T., Giglio, L., Leeuwen, T. T. van, Chen, Y., Rogers, B. M., Mu, M., Marle, M. J. E. van, Morton, D. C., Collatz, G. J., Yokelson, R. J., and Kasibhatla, P. S.: Global fire emissions estimates during 1997–2016, 9, 697–720, https://doi.org/10.5194/essd-9-697-2017, 2017.

Williams, C. A., Collatz, G. J., Masek, J., and Goward, S. N.: Carbon consequences of forest disturbance and recovery across the conterminous United States, 26, https://doi.org/10.1029/2010GB003947, 2012.

Winkler, A. J., Myneni, R. B., Hannart, A., Sitch, S., Haverd, V., Lombardozzi, D., Arora, V. K., Pongratz, J., Nabel, J. E. M. S., Goll, D. S., Kato, E., Tian, H., Arneth, A., Friedlingstein, P., Jain, A. K., Zaehle, S., and Brovkin, V.:

Slowdown of the greening trend in natural vegetation with further rise in atmospheric CO_2, 18, 4985–5010, https://doi.org/10.5194/bg-18-4985-2021, 2021.

Woodbury, P. B., Smith, J. E., and Heath, L. S.: Carbon sequestration in the U.S. forest sector from 1990 to 2010, 241, 2007.

Zhang, Y., Yao, Y., Wang, X., Liu, Y., and Piao, S.: Mapping spatial distribution of forest age in China, 4, 108–116, https://doi.org/10.1002/2016EA000177, 2017.

Zhu, Z., Piao, S., Myneni, R. B., Huang, M., Zeng, Z., Canadell, J. G., Ciais, P., Sitch, S., Friedlingstein, P., Arneth, A., Cao, C., Cheng, L., Kato, E., Koven, C., Li, Y., Lian, X., Liu, Y., Liu, R., Mao, J., Pan, Y., Peng, S., Peñuelas, J., Poulter, B., Pugh, T. A. M., Stocker, B. D., Viovy, N., Wang, X., Wang, Y., Xiao, Z., Yang, H., Zaehle, S., and Zeng, N.: Greening of the Earth and its drivers, 6, 791–795, https://doi.org/10.1038/nclimate3004, 2016.

Zscheischler, J., Mahecha, M. D., Avitabile, V., Calle, L., Carvalhais, N., Ciais, P., Gans, F., Gruber, N., Hartmann, J., Herold, M., Ichii, K., Jung, M., Landschützer, P., Laruelle, G. G., Lauerwald, R., Papale, D., Peylin, P., Poulter, B., Ray, D., Regnier, P., Rödenbeck, C., Roman-Cuesta, R. M., Schwalm, C., Tramontana, G., Tyukavina, A., Valentini, R., Werf, G. van der, West, T. O., Wolf, J. E., and Reichstein, M.: Reviews and syntheses: An empirical spatiotemporal description of the global surface–atmosphere carbon fluxes: opportunities and data limitations, 14, 3685–3703, https://doi.org/10.5194/bg-14-3685-2017, 2017.